Heliyon 9 (2023) e12948

Contents lists available at ScienceDirect

Heliyon

journal homepage: www.cell.com/heliyon

Research article

Novel N-benzyl-2-oxo-1,2-dihydrofuro [3,4-d]pyrimidine-3 (4H)-carboxamide as anticancer agent: Synthesis, drug-likeness, ADMET profile, DFT and molecular modelling against EGFR target

Ayşen Şuekinci Yılmaz *, Gühergül Uluçam

Chemistry Department, Faculty of Science, Trakya University, 22030, Edirne, Turkey

ARTICLE INFO

Keywords:
Curtius rearrangement
DU145
HT29
HOMO-LUMO
B3LYP

ABSTRACT

A novel compound N-benzyl-2-oxo-1,2-dihydrofuro [3,4-d]pyrimidine-3(4H)-carboxamide (DHFP) was synthesized by addition, rearrangement, and intramolecular cyclization reactions. The three-dimensional geometry of DHFP has been determined by density functional theory calculations in the gas phase. Thus, the geometrical properties of DHFP such as the bond lengths, bond angles, and dihedral bond angles have been determined in the optimized molecular configuration. Also, the HOMO-LUMO energies were calculated. The charge distribution of the DHFP has been calculated by Natural Population Analysis (NPA) approach. NMR and FTIR spectra were calculated and compared with their experimental corresponding to confirm the synthesis of the DHFP. The anticancer activities of the DHFP were also determined on human colon cancer (HT29) and prostate cancer (DU145) cell lines. Molecular docking studies of the DHFP with EGFR tyrosine kinase, which is responsible for cancer cell proliferation and growth, were performed and it was observed that docking interaction took place. The DHFP has the potential to be a drug, as it is determined that DHFP obeys Lipinski's five rules, can cross the blood-brain barrier, and can be rapidly absorbed from the gastrointestinal wall.

1. Introduction

Pyrimidine, an important nitrogen-containing aromatic heterocyclic compound, is found in the structure of DNA and RNA, which carry the necessary information for life. Many different pyrimidine compounds have been first designed, and then synthesized, and it has been seen that they have quite a lot of biological effects such as anti-proliferative [1], antiviral [2], antitumor [3], anti-inflammatory [4], antibacterial [5], antifungal [6], anti-β-glucuronidase [7]. Also, its anti-Alzheimer [8] and anti-tuberculosis [9] effects have been identified. In addition, the main component of commercial cancer drugs such as cytarabine [10], gemcitabine [11], xeloda [12], and 5-fluorouracil [13] are pyrimidine compounds.

Furopyrimidines are fused ring-containing compounds synthesized by forming a pyrimidine ring on the furan ring by various reactions. In addition, these compounds have many biological properties similar to pyrimidines and have; therefore, been the subject of much research in recent years [14-16]. However, the concerning literature has just a few articles targeting quantum chemical calculations and molecular docking studies on furopyrimidines.

Hossam et al. have published that the anilino-furo [2,3-d]pyrimidine derivatives they synthesized have EGFR tyrosine kinase

* Corresponding author. Chemistry Department, Faculty of Science, Trakya University, 22030, Edirne, Turkey.
E-mail address: aysensuekinci@trakya.edu.tr (A. Şuekinci Yılmaz).

https://doi.org/10.1016/j.heliyon.2023.e12948
Received 17 November 2022; Received in revised form 6 January 2023; Accepted 10 January 2023
Available online 14 January 2023

inhibitory and anti-cancer effects [17]. Han et al. stated that the chiral 6-aryl-furo [2,3-d]pyrimidine-4-amines they synthesized are equipotent to Erlonitib, which is an EGFR tyrosine kinase inhibitor and is used as an anticancer drug [18]. The other study group has shown that polysubstituted thieno [2,3-d]pyrimidine derivatives have EGFR tyrosine kinase inhibitory effect with an IC_{50} value similar to that of the commercial drug Olmitinib [19]. All these studies are for the furo [2,3-d]pyrimidine skeleton, and we could not find any studies for the furo [3,4-d]pyrimidine skeleton. In this context, we synthesized the new N-benzyl-2-oxo-1,2-dihydrofuro [3,4-d] pyrimidine-3(4H)-carboxamide (DHFP) compound and investigated its EGFR kinase inhibitory and anticancer effect.

Herein, the DHFP geometry has been optimized using density functional theory (DFT) in this study. Vibrational frequencies and structural parameters.of DHFP have been obtained with the Gaussian G09w program [20]. FTIR and NMR have been calculated and compared with the experimental value. The anticancer activities have been investigated in two cell lines (prostate and colon), respectively. Molecular docking studies of compound DHFP with EGFR tyrosine kinase have been performed to evaluate its potential as an anticancer agent. Finally, data on the pharmacokinetic and drug-likeness of DHFP have been obtained using the Swiss ADME [21], and ADMET-SAR programs [22].

2. Materials and methods

2.1. Instruments and reagents

NMR spectra were recorded on Varian Mercury Plus 400 MHz spectrometer at 400 MHz for ^{1}H NMR and 100 MHz for ^{13}C NMR. ^{13}C and ^{1}H NMR spectra were taken using acetone-d6 (for 4-((3-benzylureido)methyl)furan-3-carbonyl azide) (3) and DMSO-d6 (for DHFP) as a solvent. Infrared spectra were recorded on Perkin Elmer FTIR/FIR Spectrophotometer Frontier. All high-resolution mass spectra (HRMS) were measured on UPLC-UHR-Q/TOFABSCIEX Triple TOF 4600. Uncorrected melting points were determined on the Electrothermal melting point analyzer.

4-(isocyanatomethyl)furan-3-carbonyl azide was used as starting material and was synthesized according to the Yılmaz et al. procedure [23]. The chemicals used in the experiments were obtained from commercial sources. All reactions were monitored by TLC (Thin Layer Chromatography) with Merck 0.2 mm silica gel 60 F254 aluminum plates, and silica gel (Merck 70-230 mesh) was used in column chromatography.

2.2. Theoretical method

Molecular configuration and geometrical calculations of DHFP were performed in the Gaussian G09w package program with the basis set of 6-311++G (2d, p) by using the B3LYP theory, which consists of Becke's three-parameter hybrid variable function and Lee-Yang-Parr's correlation function [24-28]. Frontier molecular orbitals and molecular electrostatic potential maps were calculated by the density functional theory B3LYP/6-311++G (2d, p) method. Gauge invariant atomic orbitals (GIAO) method was used for ^{1}H and ^{13}C NMR chemical shifts relative to reference tetramethyl silane (TMS) [29]. Since the experimental data were obtained in dimethyl sulfoxide (DMSO), theoretical calculations were made in DMSO for comparison. To reduce the theoretical errors in the spectrum, the FTIR parameters were multiplied by 0.9613 and a detailed potential energy distribution (PED) analysis was performed using the VEDA program [30]. Visualization of all data was performed in Gauss View 5.0 [20,31–33].

2.3. Anticancer activity

Anticancer activity studies of DHFP were performed on HT29 and DU145 cell lines according to our previous study [34] using the MTT (3-(4,5-Dimethylthiazol-2-yl)-2,5-diphenyl tetrazolium bromide) method [35] at the Trakya University Technology Research Development Application and Research Center (TUTAGEM).

Cell viability and cell death were calculated as follows:

$$Cell\ Viabilty\ \% = \frac{sample\ absorbance}{control\ absorbance}\ x100$$

$$Cell\ Death\ \% = 100 - Cell\ Viability\ \%$$

2.4. Molecular docking

Since many *in vivo* and *in vitro* experiments are required, it is very difficult to determine whether the synthesized compounds have biological effects. Molecular docking calculation of ligand-receptor interactions provides us with easier information about the bioactivity of the compound [36-40]. By choosing the lowest energy interaction among the molecular docking results, the best ligand-receptor interaction can be examined. Molecular docking studies were performed with Auto Dock Tools 1. 5. 6 [41,42]. Molecular docking of DHFP with EGFR tyrosine kinase was studied. The 3D crystal structure of EGFR tyrosine kinase was taken from Protein Data Bank (PDB ID:1M17) [43,44]. Water molecules were removed, and polar hydrogens and Kollman United charges were added as the biomolecule was prepared for docking. The DHFP was made ready for use for docking by minimizing its energy at the Gaussian 09w program. Partial charges of DHFP were calculated by Geistenger Method. In grid preparation, the grid box was set as $126 \times 126 \times 126$ Å for x,y and z, respectively with a grid spacing of 0.375 Å and the grid center was set to 23.55, 9.53, 58.35 for x, y

and z, respectively. Autodock docking studies were examined by using the Lamarckian Genetic Algorithm (LGA). As a result of the calculations, the lowest energy interaction was selected and the results were interpreted. All of the ligand-protein interactions were illustrated using Pymol [45,46] and Chimera software [47]. PLIP (Protein-Ligand Interaction Profiler) web tool was used to show the H bonds in detail [48].

2.5. Determinations of the data of ADME and ADMET SAR

Evaluation of the bioavailability of compounds using computer-based programs is important in the discovery and development of new drugs. The Lipinski rule assists in categorizing compounds as drug-like and non-drug like by evaluating various parameters (Hydrogen Bond Acceptor, Hydrogen Bond Donor, molecular weight, lipophilicity (log P)) [49]. Physicochemical and pharmacokinetic properties of DHFP obtained by utilizing Swiss ADME http://www.swissadme.ch/index.php free website (Swiss Institute of Bioinformatics, Switzerland) [21]. ADMET (absorption, distribution, metabolism, elimination, toxicity) is an essential part of drug discovery and gives information about the drug's behavior in metabolism. ADMET features of DHFP were obtained using the online database ADMETSAR, http://lmmd.ecust.edu.cn/admetsar2 [50].

3. Result and discussion

3.1. Synthesis of DHFP

Synthesis of N-benzyl-2-oxo-1,2-dihydrofuro [3,4-d]pyrimidine-3(4H)-carboxamide (DHFP) consists of three steps as shown in Fig. 1: The first step is the addition of benzylamine (2) to the isocyanate on 4-(isocyanatomethyl)furan-3-carbonyl azide (1). The second step involves the conversion of the azide group on 4-((3-benzylureido)methyl)furan-3-carbonyl azide (3) to isocyanate (intermediate state) by the Curtius rearrangement reaction. The reaction continued without isolating the intermediate product (4) in the second step. The third step is the synthesis of DHFP by the intramolecular cyclization reaction of 1-benzyl-3-((4-isocyanatofuran-3-yl) methyl)urea (4).

3.1.1. Synthesis of 4-((3-benzylureido)methyl)furan-3-carbonyl azide (3)

0.22 g (1.15 mmol) of 4-(methylisocyanate)furan-3-carbonyl azide (1) was dissolved in 10 mL of dry benzene, 0.14 mL (0.14 g, 1.27 mmol) of benzylamine (2) was added and then stirred at room temperature under nitrogen atmosphere. According to the TLC result, the reaction was finished after 5 min. The precipitate was filtered, and the crude product was purified by column chromatography in a 1:1 ethylacetate: hexane solvent system. 0.43 g 4-((3-benzylureido)methyl)furan-3-carbonyl azide (6) (94%) was obtained as white crystals. Mp: 95.3–97.1 °C, ^{1}H NMR (400 MHz, acetone-d6) δ (ppm): 8.23 (s, 1H, =CH), 7.58 (s, 1H, =CH), 7.2–7.3 (m, 5H, =CH), 6.08 (br. s, 1H, NH), 5.91 (br. s, 1H, NH), 4.39 (d, 2H, CH_2), 4.32 (d, 2H, CH_2), ^{13}C NMR (100 MHz, acetone-d6) δ (ppm): 172.9 (CON_3), 157.7 (NCON), 150.6 (=CH), 143.0 (=CH),128.1 (=CH), 127.1 (2C, =CH), 126.5 (2C, =CH), 124.2 (=C), 119.4 (=CH),119.0 (=C), 43.4 (CH_2), 33.7 (CH_2), FAR FTIR (cm-1): 3316 (broad, –NH), 2153 (-N_3) 1687 (NCON), 1662 (CON_3), LC-Q/TOF (exp.) ($C_{14}H_{13}O_3N_5$ (+Na)): 322.0937, LC-Q/TOF (theo.) ($C_{14}H_{13}O_3N_5$ (+Na)): 322.0916.

3.1.2. Synthesis of N-benzyl-2-oxo-1,2-dihydrofuro [3,4-d]pyrimidine-3(4H)-carboxamide (DHFP)

0.19 g (0.64 mmol) of 4-((3-benzylureido)methyl)furan-3-carbonyl azide (3) was refluxed in 15 mL of dry THF under nitrogen atmosphere for 16 h. The solvent was evaporated, and the crude product was purified by column chromatography of the 2:3 Ethyl acetate/Hexane solvent system. 0.124 g (73.3%) of N-benzyl-2-oxo-1,2-dihydrofuro [3,4-d]pyrimidine-3(4H)-carboxamide (DHFP) was obtained as a white shiny solid. Mp: 218.6–220.1 °C,^{1}H NMR (400 MHz, DMSO-d6) δ (ppm): 9.93 (s, 1H, NH), 9.49 (s, 1H, NH), 7.45 (s, 1H, =CH), 7.31 (s, 1H, =CH), 7.24–7.33 (m, 5H, =CH), 4.77 (s, 2H, CH_2), 4.77 (d, 2H, CH_2),^{13}C NMR (100 MHz, DMSO-d_6) δ (ppm): 155.2 (C]O), 153.4 (C]O), 139.5 (=CH), 137.0 (=C), 128.8 (=C), 127.6 (=C), 127.3 (2C,=CH), 125.3 (2C,=CH), 124.0(=CH), 109.5 (=C), 43.9 (CH_2), 39.3 (CH_2),LC-Q/TOF (exp.) ($C_{14}H_{14}O_3N_3$(+H)): 272.1035, LC-Q/TOF (theo.) ($C_{14}H_{14}O_3N_3$(+H)): 272.1035.

Experimental ^{1}H and ^{13}C NMR, FTIR and Q-TOF spectrum data of **3** and DHFP was also given as supplementary data.

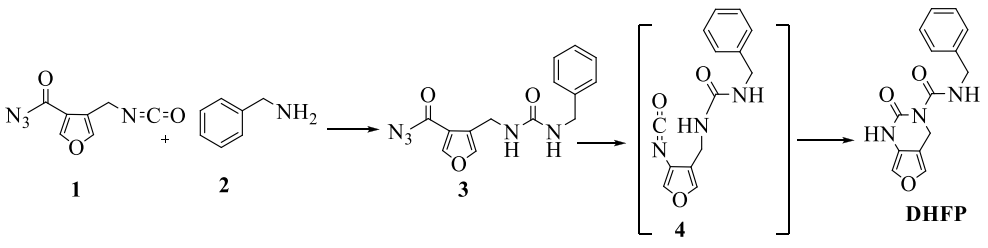

Fig. 1. Synthesis of DHFP.

3.2. Molecular geometry

DFT/B3LYP/6-311++G (2d, p) method is employed to obtain the geometry of the DHFP by calculating its minimized energy. The molecular geometry of the DHFP is shown in Fig. 2. The parameters for structural analysis such as selected bond lengths, bond angles, and dihedral bond angles are given in Table 1.

The calculated NMR and FTIR spectra are compared with those of experimental spectra to be able to confirm the theoretically obtained geometry of the DHFP for its minimized energy.

The charge distribution in the atoms in the molecule is important for determining the electrostatic interaction and molecular force fields [51,52]. The atomic charge distribution of the DHFP is obtained by Natural Population Analysis (NPA) method within the framework of Gaussian 09 and listed in Table 2. The atomic charge distribution shows that the negative charges localize on the electronegative oxygen and nitrogen atoms, while the positive charges are on the hydrogen atoms in the molecule. Carbon atoms can have negative or positive charges with respect to the electronegative atoms around them. The highest negative charges were found as −0.33848 and −0.33840 on O10 and O12 atoms, respectively. As expected, the highest positive charges were found as 0.42333 and 0.42106 on C8 and C11 atoms, respectively. Since there are three electronegative atoms, two nitrogen, and one oxygen, to which each is bonded, the carbon atoms in question become electron-depleted and positively charged.

Atomic charge distribution calculations were also performed using the MPA method. However, the results found with NPA were more consistent than those found with MPA. For example, in the distribution obtained with MPA, the highest positive charges were not found on C8 and C11.

3.3. Experimental and theoretical ^{13}C NMR and ^{1}H NMR chemical shift values

Experimental and theoretical ^{1}H NMR and ^{13}C NMR chemical shift values of DHFP as converted from Hertz units to ppm are listed in Table 3 referencing TMS. The experimental NMR values were taken in DMSO-d6 solvent while theoretical NMR data were calculated in the gas phase and again in DMSO solvent. Eleven hydrogen atoms in the DHFP structure give seven proton NMR signals and can be classified as two hydrogens attached to aliphatic carbons, three hydrogens attached to aromatic carbons, and two hydrogens attached to amines. As expected, ^{13}C NMR shows twelve different carbons in aliphatic, aromatic, and carbonyl structures.

The two identical benzylic protons (CH_2) give a doublet peak because of the spin-spin interaction of protons in H_2C–NH. Experimentally, these protons were observed as a doublet at 4.39 ppm, while theoretically they (H28 and H27) were seen as two separate peaks at 3.82 and 5.27 ppm. The aliphatic identical protons in the CH_2 of the pyrimidine ring have a single peak because there is no H on its neighboring atoms. Their experimental corresponding was at 4.77 ppm as a singlet, while the theoretical values of H23 and H24 were at 4.32 and 5.90 ppm, respectively.

Two different aromatic protons of the furan ring give a singlet for each because of the absence of H in their neighboring atoms. The experimental values of furan ring protons, namely H22 and H21 were at 7.31 and 7.45 ppm, whereas their theoretical values were at 7.18 and 7.35 ppm, respectively. The five protons on the ortho (H33, H29), meta (H32, H30), and para (H31) positions of the benzene ring give three different peaks. The signals were split due to the neighboring hydrogen atoms in carbons. While the experimental values of these protons were observed as multiplet in the range of 7.24–7.33 ppm, the theoretical values were 7.58 ppm for H33 and H31, 7.64 ppm for H32 and H30, and 7.98 ppm for H29.

The amine protons must appear as a broad singlet. Indeed, the experimental values of protons of two amines were at 9.49 and 9.93 ppm as a broad singlet, their (H25 and H26) theoretical values were at 6.03 and 9.59 ppm, respectively.

Considering the ^{13}C NMR spectra of the DHFP, the experimental values of the aliphatic carbon on the pyrimidine ring (CH_2) and benzylic carbon peak (CH_2) were at 39.31 and 43.98 ppm, while the theoretical values of C6 and C14 were at 41.30 and 46.35 ppm,

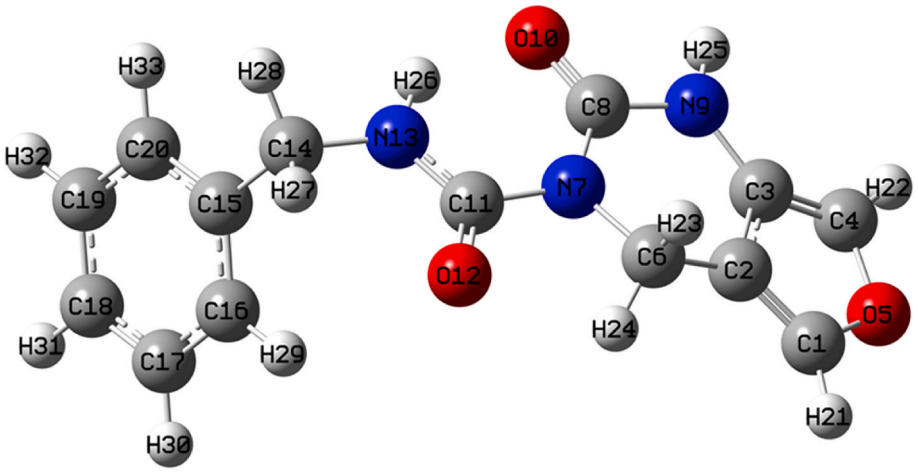

Fig. 2. Molecular configuration of DHFP.

Table 1
Theoretical bond lengths (Å), bond angles (∘), and dihedral bond angles (∘) of DHFP in the gas phase. Labels refer to Fig. 2.

Selected Bond Lengths (Å)		Selected Bond Angles (°)		Selected Dihedral Bond Angles (°)	
C1–C2	1.355	C1–O5–C4	107.503	C1–O5–C4–H22	179.236
C1–O5	1.361	C1–C2–C3	105.871	C1–O5–C4–C3	0.521
C2–C3	1.420	C3–C4–H22	134.650	O5–C4–C3–C2	−0.213
C1–H21	1.076	C3–N9–H25	120.953	C1–C2–C3–N9	178.854
C2–C6	1.488	C3–N9–C8	122.632	C2–C3–N9–C8	−20.053
C6–N7	1.489	N9–C8–N7	116.753	C3–N9–C8–O10	−163.966
N7–C8	1.392	N9–C8–O10	118.727	N9–C8–N7–C11	−175.940
C8–N9	1.382	C8–N7–C6	122.352	O10–C8–N7–C11	3.858
C8–O10	1.227	N7–C11–N13	117.046	C8–N7–C11–O12	−178.800
C3–N9	1.390	N7–C11–O12	118.482	C8–N7–C11–N3	1.251
C6–H28	1.096	C11–N13–H26	117.088	O12–C11–N13–H26	179.726
N9–H25	1.009	C11–N13–C14	121.582	O12–C11–N13–C14	−1.631
C11–N7	1.442	H27–C14–H28	107.980	N13–C14–C15–C16	74.990
C11–O12	1.222	C14–C15–C16	120.433	C14–C15–C16–C17	−179.394
C11–N13	1.345	C15–C16–C17	120.484	C15–C16–C17–C18	−0.178
N13–H26	1.015	H29–C16–C17	120.226	H29–C16–C17–H30	0.176
C14–N13	1.460				
C14–H27	1.090				
C14–C15	1.516				
C15–C16	1.398				
C16–C17	1.390				
C17–C18	1.393				
C16–H29	1.084				
C17–H30	1.084				

Table 2
Natural Charges of DHFP. Atomic labels refer to Fig. 2.

Atoms	NPA	Atoms	NPA
C1	0.07788	N7	−0.27129
C2	−0.07397	N9	−0.30476
C3	0.03910	N13	−0.32219
C4	0.03988	H21	0.09986
C6	−0.08963	H22	0.09985
C8	0.42333	H23	0.10259
C11	0.42106	H24	0.12582
C14	−0.09479	H25	0.20563
C15	−0.02409	H26	0.21789
C16	−0.09702	H27	0.11421
C17	−0.09703	H28	0.09860
C18	−0.10163	H29	0.10934
C19	−0.09876	H30	0.10143
C20	−0.09957	H31	0.10148
O5	−0.22750	H32	0.10138
O10	−0.33848	H33	0.09980
O12	−0.33840		

respectively. The eight aromatic carbon peaks were experimentally in the range of 109.51–139.55 ppm, as they theoretically were in the range of 127.33–148.39 ppm. Experimentally, the pyrimidine ring carbonyl carbon C8 was at 153.41 ppm, and the aliphatic carbonyl carbon C11 was at 155.22 ppm. Meanwhile, their theoretical corresponding values of C8 and C11 were at 159.73 and 160.06 ppm, respectively. The agreement between the experimental and theoretical NMR results points out that the DHFP was synthesized successfully while theoretical calculations confirm the molecular structure of the DHFP.

3.4. Experimental and theoretical vibration frequencies

The experimental vibration values were obtained by Perkin Elmer FTIR/FIR Spectrophotometer Frontier, while theoretical vibrations were calculated using DFT/B3LYP method and the 6-311++G (2d, p) basis set. The structure of DHFP contains 33 atoms which theoretically gave 93 normal vibrational modes. The experimental and theoretical FTIR spectra of DHFP, shown in Fig. 3, were analyzed based on characteristic peaks such as amine, aromatic, carbonyl, and CH_2 vibrations. In addition, the experimental FTIR frequencies are listed in Table 4 together with their corresponding calculated values. The theoretical data in the table also reflects the details of the percentage potential energy distribution (PED) and vibrational mode assignments. The experimental and theoretical vibrational spectra are found to be compatible.

Table 3
The experimental and theoretical ^{1}H NMR and ^{13}C NMR chemical shift values of DHFP according to TMS δ/ppm (s: singlet, br.: broad, m: multiplet, Assign.: assignments). The hydrogen and carbon labels can be followed from Fig. 2.

^{1}H NMR				
Experimental		Theoretical		
Assign.	δ (ppm)	Assign.	Gas phase	DMSO
CH_2	4.38 (d)	H28	3.58	3.82
		H27	5.39	5.27
CH_2	4.77 (s)	H23	4.17	4.32
		H24	5.98	5.90
CH (arom., 5H)	7.24–7.33(m)	H33	7.35	7.58
		H31	7.40	7.58
		H32	7.47	7.64
		H30	7.51	7.64
		H29	8.03	7.98
CH (arom.)	7.31 (s)	H22	6.99	7.18
CH (arom.)	7.45 (s)	H21	7.21	7.35
NH	9.49 (br. s)	H25	5.54	6.03
NH	9.93 (br.s)	H26	9.49	9.59
^{13}C NMR				
Experimental		Theoretical		
Assign.	δ (ppm)	Assign.	Gas phase	DMSO
CH_2	39.31	C6	40.93	41.30
CH_2	43.99	C14	46.76	46.35
C (arom.)	109.51	C2	116.22	116.06
CH (arom.)	124.02	C18	131.18	131.51
CH (arom.)	125.35	C16	134.54	133.96
		C20	132.06	132.88
CH (arom.)	127.32	C17	133.03	132.06
		C19	132.01	132.71
C (arom.)	127.64	C3	132.45	132.19
C (arom.)	128.81	C15	147.91	148.39
CH (arom.)	137.04	C1	141.28	141.85
CH (arom.)	139.55	C4	125.80	127.33
C=O	153.41	C8	158.60	159.73
C=O	155.22	C11	158.95	160.06

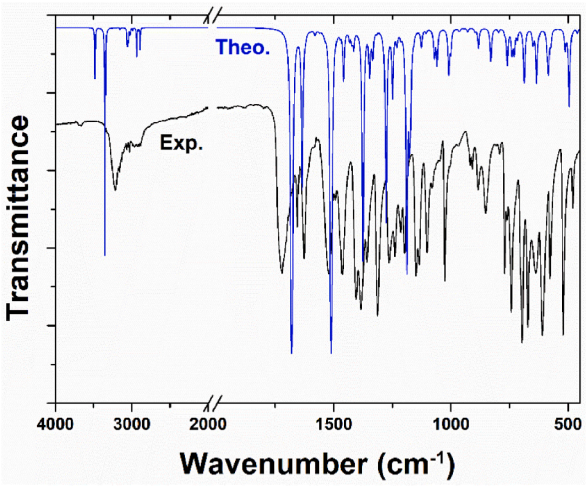

Fig. 3. Experimental and theoretical FTIR spectrum of DHFP.

3.4.1. NH vibrations

The stretching vibrations of the amide NH bond observe around 3300-3600 cm^{-1} [53–55]. In the DHFP, N9H25 and N13H26 stretching vibrations were theoretically observed at 3483 and 3351 cm^{-1}, as seen experimentally at 3623 and 3486 cm^{-1}. Furthermore, H25N9C3 and H26N13C14 in-plane bending vibrations were observed theoretically at 1511 and 1415 cm^{-1} and experimentally at 1622 and 1402 cm^{-1}. The H25N9C3C2 torsional vibration was observed theoretically at 511 cm^{-1} and experimentally at 523 cm^{-1}.

Table 4
Experimental and theoretical FTIR values of DHFP (cm^{-1}) (selected). The atom labels can be followed from Fig. 2.

Exp.	Theo.		Vibration assignment (PED)
	Unscaled	Scaled	
3694	3623	3483	νN9H25 (100)
3652	3486	3351	νN3H26 (99)
3226	3286	3159	νC4H22 (95)
3158	3271	3144	νC1H21 (95)
3061	3186	3063	νC16H29, νC17H30, νC18H31, νC19H32 (93)
–	3178	3055	νC16H29, νC17H30, νC18H31, νC19H32 (96)
–	3170	3047	νC16H29, νC17H30, νC18H31, νC19H32 (87)
3042	3160	3038	δ_C16C17C18 (87)
3023	3151	3029	νC20H33 (77)
–	3140	3018	νC6H24 (98)
2965	3109	2989	νC14H27 (80),
			νC14H28 (20)
2926	3054	2936	νC14H27 (20),
			νC14H28 (80)
2888	3010	2894	νC6H23 (98)
1723	1747	1679	νC8O10, νC11O12 (63),
			νN3C11 (11)
1654	1701	1635	νC8O10, νC11O12 (66)
1622	1572	1511	νN13C11 (18),
			δ_H26N13C14 (58)
1522	1516	1457	δ_H24C6H23 (72)
1465	1490	1432	δ_H31C18C19, δ_H27C14C15, δ_H30C17C18, δ_H32C19C20 (55)
	1480	1423	δ_H28C14H27 (91)
1402	1472	1415	δ_H25N9C3 (31)
1383	1431	1376	νC1C2, νC2C6, νN7C8 (34),
			δ_H24C6H23 (15)
1358	1402	1348	νC3C4 (15),
			δ_H25N9C3 (26)
1308	1388	1334	τH27C14C15C16, τH28C14C15C16 (80)
1264	1328	1277	νN9C8 (13),
			δ_H21C1O5, δ_H22C4O5 (35)
1239	1299	1249	δ_H23C6C2 (40)
1214	1280	1230	νC15C20, νC16C17, νC17C18 (12),
			δ_H27C14C15, δ_H29C16C17, δ_H33C20C19 (13) τH28C14C15C16 (26),
1195	1236	1188	νC3C4 (13)
1151	1225	1178	νC14C15 (18),
			νN13C11 (10)
1132	1220	1173	νC14C15 (20),
			δ_H29C16C17, δ_H30C17C18, δ_H32C19C20, δ_H33C20C19 (10)
1101	1171	1126	νO5C1, νO5C4 (14),
			δ_C6C2C1 (13),
			δ_C3C4O5, δ_C1O5C4 (12)
1082	1114	1071	νC15C20, νC17C18 (11),
			δ_H27C14C15, δ_H29C16C17, δ_H33C20C19 (21)
1025	1102	1059	νN13C14 (10)
–	1050	1009	νO5C1, νO5C4 (58),
			δ_H21C1O5 δ_H22C4O5 (14)
968	1041	1001	νN13C14 (23),
886	918	882	δ_C3C4O5 (12),
			δ_C1O5C4 (52)
848	863	830	δ_C1O5C4 (18),
			δN7C11N13, δN9C8O10 (10)
746	790	759	τC2C1O5C4, τC1O5C4C3 (15),
			τH21C1O5C4 (63)
741	769	739	δ_C16C17C18, δ_C18C19C20, δ_C17C18C19 (10) τH31C18C19C20, τH32C19C20C15, τH33C20C19C18 (20), γO12N13N7C11 (41)
–	759	730	γO10N9N7C8 (82)
699	714	686	τH31C18C19C20, τH32C19C20C15, τH33C20C19C18 (45)
667	713	685	τH22C4O5C1 (40)
642	676	650	δ_C6C2C1 (17),
			δN7C11N13, δN9C8O10 (13)
611	660	634	τH26N13C11N7 (76)
579	608	585	δO12C11N13 (14),
			τC2C1O5C4, τC1O5C4C3 (58)
523	532	511	τH25N9C3C2 (40)
479	515	495	τH25N9C3C2 (28)

Experimental: exp., theoretical: theo., PED: potential energy distribution, ν: stretching, δ: in-plane bending, γ: out-of-plane bending, τ: torsion.

3.4.2. Aromatic CH vibrations

Aromatic CH bond stretching vibrations are usually just over 3000 cm^{-1} [54,56]. There are seven aromatic CH on the DHFP structure, and their vibrational values were very close to each other. These CH stretching vibrations were theoretically observed in the range of 3029-3159 cm^{-1}, and experimentally in the range of 3023-3226 cm^{-1}, respectively. These atoms in-plane bending vibrations of these atoms theoretically observed in the range of 1432-1537 cm^{-1} while they were experimentally in the range of 1465-1622 cm^{-1}.

3.4.3. Carbonyl vibrations

Depending on the electronegative atoms attached to the carbonyl group, the carbonyl group gives a stretching vibration in the range of 1650-1800 cm^{-1} [53,54,57]. There are two different carbonyl groups in the DHFP structure, but since both are located between N–N they gave the same experimental and theoretical vibrations value. While C8O10 and C11O12 stretching frequencies were theoretically at 1679 cm $^{-1}$, experimentally at 1723 cm^{-1}. In addition, N9C8O10 and O12C11N13 in-plane bending vibrations were theoretically observed at 650 and 585 cm^{-1}, and experimentally at 642 and 579 cm^{-1}.

3.4.4. CH_2 vibrations

The characteristic vibration of the CH_2 is the stretching vibration in the range of 2900-3000 cm^{-1} and the in-plane bending vibration around 1450 cm^{-1} [58]. The C6H23, C6H24, C14H27 and C14H28 stretching vibrations were observed theoretically in the range of 2894-3018 cm^{-1}, and experimentally in the range of 2888-2965 cm^{-1}. In-plane bending vibration of these atoms was observed theoretically at 1376, 1423 and 1432 cm^{-1} and experimentally at 1383 and 1465 cm^{-1}.

3.5. HOMO-LUMO analysis and electronic properties

Frontier Molecular Orbital (FMO) deals with the calculation of the highest occupied molecular orbital (HOMO) and the lowest unoccupied molecular orbital (LUMO) energy levels. Thus, information about the reactivity and physical properties of the molecule is obtained. HOMO indicates the electron-donating ability and is used to calculate the Ionization Potential (IP), while LUMO refers to the electron-accepting ability and is used for the calculation of Electron Affinity (EA). The energy difference between HOMO and LUMO tells us a lot about molecules. If the energy difference between two orbitals is less, the molecule is more polarized, with high softness, low hardness, and high chemical reactivity [52,59–61]. If the energy difference between two orbitals is large, they are vice versa.

The HOMO and LUMO energies of the DHFP were calculated using the B3LYP theory and the 6-311++G (2d, p) base set. The molecular orbitals for the calculated HOMO and LUMO energies are shown in Fig. 4. Here Gaussian output values in the atomic unit (a.u.), were converted to electrostatic units (1 a.u. = 27.2116 eV) [62,63].

The Ionization Potential (IP), Electron Affinity (EA), Electronegativity (χ), Chemical Potential (μ), Chemical Hardness (η), and

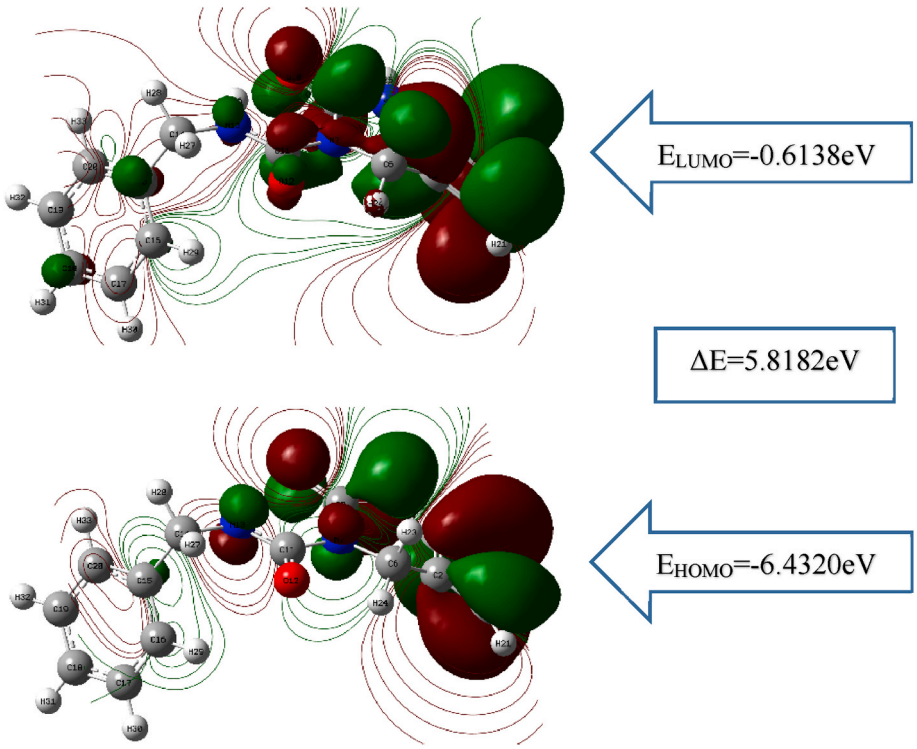

Fig. 4. HOMO and LUMO energy levels for DHFP.

Chemical Softness (s) for DHFP were calculated using HOMO and LUMO values. Molecular electrical properties were obtained by using HOMO and LUMO energies and the results were given in Table 5. In summary, the low value of ΔE, calculated as 5.8182 eV, proves the high chemical reactivity of the DHFP molecular structure.

3.6. Molecular electrostatic potential surface

The molecular electrostatic potential (MEP) map, if calculated, shows the positive and negative regions of the molecule and allows us to gain insight into the chemical reactivity of the molecule. The MEP of DHFP calculated is shown in Fig. 5. It shows the positive parts of the molecule in blue, the negative parts in red, and the neutral parts in green [53,64–66].

When the MEP of the DHFP was examined in Fig. 5, the negative regions (red region) were found localized on the oxygen atoms as the positive regions (blue region) localized on the hydrogen atoms. This indicates possible sites for nucleophilic attack.

3.7. Anticancer activity

The cytotoxicity of the DHFP has been examined by MTT assay towards human colon cancer HT29 and prostate cancer DU145 cell lines. The dose application times were 24 h and 48 h. The cell viability percentages of HT29 and DU145 are shown depending on doses in Fig. 6A and B, respectively. In 24-h dose application on HT29 cells, the growth of cell lines remained above 50 percent on average in the x - y dose range. In the 48-h test on the same cells, there was no significant change in cell viability compared to the 24 h test. The inhibitory effects of DHFP on DU145 cells for 24 h dose application exhibited over 70% viability even for the highest dose (300 ppm). However, DHFP was effective on DU145 in 48 h application as 59.13% death was observed for 300 ppm dose. The IC_{50} value is found to be 17.4 ppm. This sharp difference between 24 h and 48 h dose application may be due to the aggressive properties of prostate cancer cells. The MTT studies have determined that DHFP showed a higher inhibition on DU145 compared to the HT29 cell line. According to these results, DHFP exhibited reasonable anticancer activity against HT29 while it showed a potent activity on DU145 cells.

To the best of our knowledge, there is no study that evaluates the anticancer effect of furo- [3,4-d] pyrimidine compounds. The closest examples are given by the two investigation of the anticancer effects of pyrimidine-based compounds on HT29 and DU145 cells [67,68]. It was seen that DHFP was effective at higher doses in comparison with the doses applied in these latter studies.

3.8. Molecular docking analysis

The epidermal growth factor receptor (EGFR) has an important role in cell growth and division. The amount of EGFR protein is above normal in some types of cancer cells such as colorectal cancer, head and neck cancer, lung cancer, and breast cancer. It causes cancer cells to divide faster and grow faster. Thus, EGFR tyrosine kinase inhibitors are used as a drug in cancer treatment [69,70].

In this context, molecular docking studies become crucial as they provide an opportunity to gain information about ligand-receptor interaction before any experimental drug test. It can be found out which region of the protein the ligand binds to, what kind of interactions it makes, and their binding energies in these docking calculations [71,72]. The molecular docking calculations of various furopyrimidine compounds have shown that they behave as an inhibitor of EGFR tyrosine kinase [17–19,73,74]. To have an idea about if the compound DHFP can carry the potential of being an inhibitor as a molecule containing furopyrimidine ring, we carried out docking calculations on its effect on EGFR tyrosine kinase (PDB ID:1M17). Amongst the calculated docking positions, the lowest energy protein-ligand binding was selected. The selected docking pose demonstrated that the binding energy of DHFP and EGFR tyrosine kinase was found to be −7.4 kcal/mol. Although this binding energy value is higher than that of the standard drug erlotinib which has been given as −10.6 kcal/mol [67], the DHFP does hydrogen bonds and hydrophobic interactions, as expected from an anticancer agent. The binding sites of DHFP to EGFR tyrosine kinase are shown in Fig. 7A from which DHFP interacts close to the binding site of erlotinib in the EGFR tyrosine kinase structure. These interactions are hydrophobic with PHE699, VAL702, and ASP831 and hydrogen bonds with ASP813 and ARG817 amino acids in EGFR tyrosine kinase, as all interactions are shown in Fig. 7B. Moreover, it is seen in Fig. 7C that N9 in the DHFP structure is both a hydrogen bond acceptor and donor in the two different interactions.

3.9. Evaluation of pharmacokinetics and drug-likeness properties of DHFP

By evaluating the pharmacokinetic, toxicity, and bioavailability properties of the compounds, their use or development as drugs can be achieved [68–70]. As shown in Table 6, DHFP follows the Lipinski rule (molecular weight ≤500, number of H bond acceptor ≤5, number of H bond donor ≤5, TPSA/A2≤140, log P ≤ 5) as a drug candidate. According to the ADME result, DHFP has a high GI (gastrointestinal) absorption value means that the drug is rapidly absorbed.

The ADMET data of the DHFP which is computationally forecasted from its given molecular structure are shown in Table 7. It is exhibited that the DHFP has oral bioavailability, is rapidly absorbed in the human intestine, and can cross the blood-brain barrier. In addition, mitochondria provide the subcellular localization of DHFP. DHFP is not a P-glycoprotein inhibitor or substrate. Since, P-glycoprotein pumps drugs back into the lumen, reducing the drug absorption, it can be said that the bioavailability and bioactivity of the DHFP is high.

4. Conclusions

Novel N-benzyl-2-oxo-1,2-dihydrofuro [3,4-d]pyrimidine-3(4H)-carboxamide was synthesized with a very good yield in the

Table 5
Electronic structure values of DHFP.

E_{HOMO}(eV)	E_{LUMO}(eV)	ΔE (eV)	IP(eV)	EA (eV)	χ (eV)	φ (eV)	η (eV)	σ (eV^{-1})
−6.4320	−0.6138	5.8182	6.4320	0.6138	3.5229	−3.5229	2.9091	0.3437

IP= Ionization Potential = -HOMO, EA = Electron Affinity = -LUMO.
χ = Electronegativity = (IP + EA)/2, φ = Chemical potential = - χ,
η = Chemical hardness = (IP-EA)/2, σ = Chemical softness = 1/η.

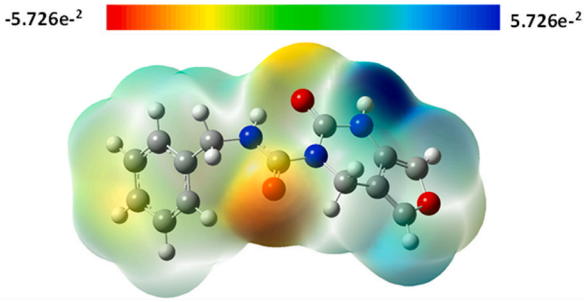

Fig. 5. Molecular electrostatic potential map for DHFP.

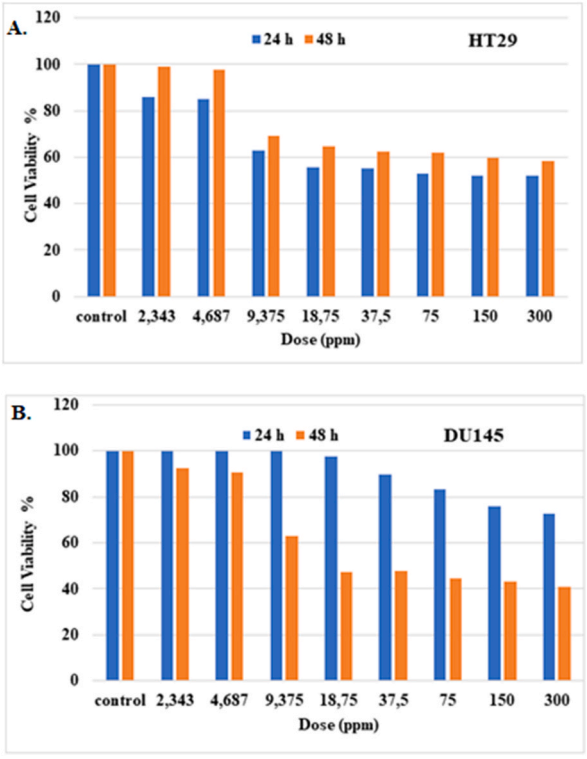

Fig. 6. A: The cytotoxic effect of DHFP on HT29 cell line, B: The cytotoxic effect of DHFP on DU145 cell line.

present study. NMR and FTIR spectra confirm the expected structure of DHFP, while the mass spectrum is 100% compatible with the calculated mass of the compound, indicating high purity. Its molecular configuration was determined theoretically by DFT calculations. DHFP bounds to EGFR tyrosine kinase near Erlotinib. Therefore, we thought that it could be a potential anticancer agent and determined effective anticancer activity in colon and prostate cancer cells. The biological properties of DHFP can be further investigated, as ADME and ADMET calculations reveal its high bioavailability. For future studies, it would be desirable to synthesize different derivatives of 1,2-dihydrofuro [3,4-d]pyrimidine and additional studies are required to determine their mechanism as a potential anticancer agent.

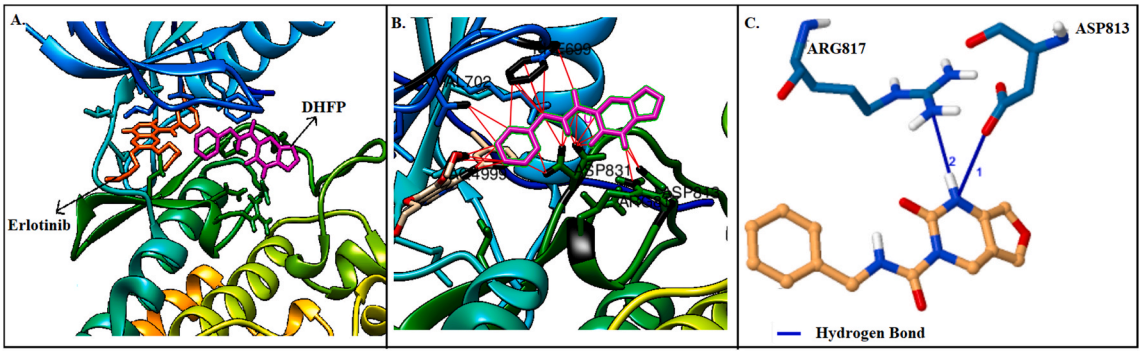

Fig. 7. A: The binding site of DHFP and erlotinib on EGFR tyrosine kinase structure, B: detailed illustration of interactions between DHFP and EGFR tyrosine kinase and C: detailed illustration of H bonds between DHFP and EGFR tyrosine kinase.

Table 6
Data of Lipinski rule, Pharmacokinetics, and Drug likeness.

Mw	NBR	HBA	HBD	TPSA/A2 (≤140)	Consensus Log $P_{o/w}$	Lipinski Rule		Bioavailability Score	GI abs.
						result	violation		
271.27	4	3	2	74.58	1.47	yes	0	0.55	High

Mw: Molecular weight, NBR: Number of rotatable bonds, HBA: Number of Hydrogen bond acceptors, HBD: Number of Hydrogen bond donors, TPSA: Topological polar surface area, Consensus Log $P_{o/w}$: Log $P_{octane/water}$, GI: Gastrointestinal.

Table 7
Pharmacokinetics and ADMET data.

Human Intestinal Absorption (<0.25 poor, >0.80 high)	Human oral bioavailability	Caco-2 (<0.25 poor, >50 great	Blood Brain Barrier	Subcellular localization	P-glycoprotein inhibitor	P- glycoprotein substrate
0.9640	yes	0.7279	yes	mitochondria	No	no

Author contribution statement

Ayşen Şuekinci Yılmaz: Conceived and designed the experiments; Performed the experiments; Analyzed and interpreted the data; Contributed reagents, materials, analysis tools or data; Wrote the paper.

Gühergül Uluçam: Conceived and designed the experiments; Analyzed and interpreted the data; Wrote the paper.

Funding statement

Dr. Ayşen Şuekinci Yılmaz was supported by Trakya Üniversitesi (TUBAP:2018/199).

Data availability statement

No data was used for the research described in the article.

Declaration of interest's statement

The authors declare no conflict of interest.

Acknowledgements

The authors are indebted to Trakya University Scientific Research Projects Coordination Unit (TUBAP 2018/199) for financial support for this work. We thank the Trakya University Technology Research Development Application and Research Center (TUTA-GEM) for the Q-TOF, FTIR, and cytotoxicity analyses.

Appendix A. Supplementary data

Supplementary data related to this article can be found at https://doi.org/10.1016/j.heliyon.2023.e12948.

References

[1] P.F. Lamie, J.N. Philoppes, Design, synthesis, stereochemical determination, molecular docking study, in silico pre-ADMET prediction and anti-proliferative activities of indole-pyrimidine derivatives as Mcl-1 inhibitors, Bioorg. Chem. 116 (2021), 105335, https://doi.org/10.1016/j.bioorg.2021.105335.

[2] W.M. Basyouni, S.Y. Abbas, K.A. El-Bayouki, R.M. Dawood, M.K. El Awady, T.H. Abdelhafez, Synthesis and antiviral screening of 2-(propylthio)-7-substituted-thiazolo [5, 4-d] pyrimidines as anti-bovine viral diarrhea virus agents, J. Heterocycl. Chem. 58 (9) (2021) 1766–1774, https://doi.org/10.1002/jhet.4307.

[3] A. Ballesteros-Casallas, M. Paulino, P. Vidossich, C. Melo, E. Jiménez, J.-C. Castillo, J. Portilla, G.P. Miscione, Synthesis of 2, 7-diarylpyrazolo [1, 5-a] pyrimidine derivatives with antitumor activity. Theoretical identification of targets, Eur. J. Med. Chem. Rep. 4 (2022), 100028, https://doi.org/10.1016/j.ejmcr.2021.100028.

[4] S.A. Abdel-Aziz, E.S. Taher, P. Lan, G.F. Asaad, H.A. Gomaa, N.A. El-Koussi, B.G. Youssif, Design, synthesis, and biological evaluation of new pyrimidine-5-carbonitrile derivatives bearing 1, 3-thiazole moiety as novel anti-inflammatory EGFR inhibitors with cardiac safety profile, Bioorg. Chem. 111 (2021), 104890, https://doi.org/10.1016/j.bioorg.2021.104890.

[5] K.D. Katariya, D.V. Reddy, Oxazolyl-pyrimidines as antibacterial and antitubercular agents: synthesis, biological evaluation, in-silico ADMET and molecular docking study, J. Mol. Struct. 1253 (2022), 132240, https://doi.org/10.1016/j.molstruc.2021.132240.

[6] A.Y. Aksinenko, T.V. Goreva, T.A. Epishina, S.V. Trepalin, V.B. Sokolov, Synthesis of bis (trifluoromethyl) pyrimido [4, 5-d] pyrimidine-2, 4-diones and evaluation of their antibacterial and antifungal activities, J. Fluor. Chem. 188 (2016) 191–195, https://doi.org/10.1016/j.jfluchem.2016.06.019.

[7] F. Ali, K.M. Khan, U. Salar, S. Iqbal, M. Taha, N.H. Ismail, S. Perveen, A. Wadood, M. Ghufran, B. Ali, Dihydropyrimidones: as novel class of β-glucuronidase inhibitors, Bioorg. Med. Chem. 24 (16) (2016) 3624–3635, https://doi.org/10.1016/j.bmc.2016.06.002.

[8] S. Manzoor, S.K. Prajapati, S. Majumdar, M.K. Raza, M.T. Gabr, S. Kumar, K. Pal, H. Rashid, S. Kumar, S. Krishnamurthy, Discovery of new phenyl sulfonyl-pyrimidine carboxylate derivatives as the potential multi-target drugs with effective anti-Alzheimer's action: design, synthesis, crystal structure and in-vitro biological evaluation, Eur. J. Med. Chem. 215 (2021), 113224, https://doi.org/10.1016/j.ejmech.2021.113224.

[9] K.S. Raju, S. AnkiReddy, G. Sabitha, V.S. Krishna, D. Sriram, K.B. Reddy, S.R. Sagurthi, Synthesis and biological evaluation of 1H-pyrrolo [2, 3-d] pyrimidine-1, 2, 3-triazole derivatives as novel anti-tubercular agents, Bioorg. Med. Chem. Lett 29 (2) (2019) 284–290, https://doi.org/10.1016/j.bmcl.2018.11.036.

[10] B. Scappini, G. Gianfaldoni, F. Caracciolo, F. Mannelli, C. Biagiotti, C. Romani, E.M. Pogliani, F. Simonetti, L. Borin, R. Fanci, Cytarabine and clofarabine after high-dose cytarabine in relapsed or refractory AML patients, Am. J. Hematol. 87 (12) (2012) 1047–1051, https://doi.org/10.1002/ajh.23308.

[11] C.J. Halbrook, C. Pontious, I. Kovalenko, L. Lapienyte, S. Dreyer, H.-J. Lee, G. Thurston, Y. Zhang, J. Lazarus, P. Sajjakulnukit, Macrophage-released pyrimidines inhibit gemcitabine therapy in pancreatic cancer, Cell Metabol. 29 (6) (2019) 1390–1399, https://doi.org/10.1016/j.cmet.2019.02.001, e6.

[12] X. Fei, J.-Q. Wang, K.D. Miller, G.W. Sledge, G.D. Hutchins, Q.-H. Zheng, Synthesis of [18F] Xeloda as a novel potential PET radiotracer for imaging enzymes in cancers, Nucl. Med. Biol. 31 (8) (2004) 1033–1041, https://doi.org/10.1016/j.nucmedbio.2004.02.006.

[13] L.M. Verissimo, I. Cabral, A.M. Cabral, G. Utzeri, F.J. Veiga, A.J. Valente, A.C. Ribeiro, Transport properties of aqueous solutions of the oncologic drug 5-fluorouracil: a fundamental complement to therapeutics, J. Chem. Therm. 161 (2021), 106533, https://doi.org/10.1016/j.jct.2021.106533.

[14] M.M. Abd El-Mageed, A.A. Eissa, A.E.-S. Farag, E.E.A. Osman, Design and synthesis of novel furan, furo [2, 3-d] pyrimidine and furo [3, 2-e][1, 2, 4] triazolo [1, 5-c] pyrimidine derivatives as potential VEGFR-2 inhibitors, Bioorg. Chem. 116 (2021), 105336, https://doi.org/10.1016/j.bioorg.2021.105336.

[15] T. Gregorić, M. Sedić, P. Grbčić, A.T. Paravić, S.K. Pavelić, M. Cetina, R. Vianello, S. Raić-Malić, Novel pyrimidine-2, 4-dione–1, 2, 3-triazole and furo [2, 3-d] pyrimidine-2-one–1, 2, 3-triazole hybrids as potential anti-cancer agents: synthesis, computational and X-ray analysis and biological evaluation, Eur. J. Med. Chem. 125 (2017) 1247–1267, https://doi.org/10.1016/j.ejmech.2016.11.028.

[16] E.Y. Ahmed, N.A.A. Latif, M.F. El-Mansy, W.S. Elserwy, O.M. Abdelhafez, VEGFR-2 inhibiting effect and molecular modeling of newly synthesized coumarin derivatives as anti-breast cancer agents, Bioorg. Med. Chem. 28 (5) (2020), 115328, https://doi.org/10.1016/j.bmc.2020.115328.

[17] M. Hossam, D.S. Lasheen, N.S. Ismail, A. Esmat, A.M. Mansour, A.N.B. Singab, K.A. Abouzid, Discovery of anilino-furo [2, 3-d] pyrimidine derivatives as dual inhibitors of EGFR/HER2 tyrosine kinase and their anticancer activity, Eur. J. Med. Chem. 144 (2018) 330–348, https://doi.org/10.1016/j.ejmech.2017.12.022.

[18] J. Han, S.J. Kaspersen, S. Nervik, K.G. Nørsett, E. Sundby, B.H. Hoff, Chiral 6-aryl-furo [2, 3-d] pyrimidin-4-amines as EGFR inhibitors, Eur. J. Med. Chem. 119 (2016) 278–299, https://doi.org/10.1016/j.ejmech.2016.04.054.

[19] T. Wang, F. Wu, L. Luo, Y. Zhang, J. Ma, Y. Hu, Efficient synthesis and cytotoxic activity of polysubstituted thieno [2, 3-d] pyrimidine derivatives, J. Mol. Struct. 1256 (2022), 132497, https://doi.org/10.1016/j.molstruc.2022.132497.

[20] R.A. Gaussian09, mj frisch, gw trucks, hb schlegel, ge scuseria, ma robb, jr cheeseman, g. Scalmani, v. Barone, b. Mennucci, ga petersson, et al., Gaussian, Inc., Wallingford CT, 1 121, 2009, pp. 150–166.

[21] A. Daina, O. Michielin, V. Zoete, SwissADME: a free web tool to evaluate pharmacokinetics, drug-likeness and medicinal chemistry friendliness of small molecules, Sci. Rep. 7 (1) (2017) 1–13, https://doi.org/10.1038/srep42717.

[22] H. Yang, C. Lou, L. Sun, J. Li, Y. Cai, Z. Wang, W. Li, G. Liu, Y. Tang, admetSAR 2.0: web-service for prediction and optimization of chemical ADMET properties, Bioinformatics 35 (6) (2019) 1067–1069, https://doi.org/10.1093/bioinformatics/bty707.

[23] A.Ş. Yılmaz, M. Kaçan, New synthesis of novel 1, 2-dihydrofuro [3, 4-d] pyrimidines, Tetrahedron 73 (31) (2017) 4509–4512, https://doi.org/10.1016/j.tet.2017.05.072.

[24] R. Qu, X. Zhang, Q. Zhang, X. Yang, Z. Wang, L. Wang, Experimental and theoretical study on IR and NMR spectra of several tetrachlorinated diphenyl sulfides, Spectrochim. Acta Mol. Biomol. Spectrosc. 81 (1) (2011) 261–269, https://doi.org/10.1016/j.saa.2011.06.008.

[25] G. Uluçam, S.E. Okan, Ş. Aktaş, G.P. Öğretmen, Characterization of dinaphthosulfoxide molecule, J. Mol. Struct. 1102 (2015) 146–152, https://doi.org/10.1016/j.molstruc.2015.08.051.

[26] D. Manikandan, J. Swaminathan, S.S. Tagore, S. Gomathi, N. Sabarinathan, M. Ramalingam, K. Balasubramani, V. Sethuraman, Crystallographic, spectral and computational studies on (S)-4-(4-aminobenzyl) oxazolidin-2-one, Spectrochim. Acta Mol. Biomol. Spectrosc. 239 (2020), 118484, https://doi.org/10.1016/j.saa.2020.118484.

[27] J. Foresman, E. Frish, Exploring Chemistry, Gaussian Inc., Pittsburg, USA, 1996.

[28] N.B. Arslan, N. Özdemir, O. Dayan, N. Dege, M. Koparır, P. Koparır, H. Muğlu, Direct and solvent-assisted thione–thiol tautomerism in 5-(thiophen-2-yl)-1, 3, 4-oxadiazole-2 (3H)-thione: experimental and molecular modeling study, Chem. Phys. 439 (2014) 1–11, https://doi.org/10.1016/j.chemphys.2014.05.006.

[29] L. Zare Fekri, M. Nikpassand, M. Goldoost, Synthesis, experimental and DFT studies on crystal structure, FT-IR, 1H, and 13C NMR spectra, and evaluation of aromaticity of three derivatives of xanthens, Russ. J. Gen. Chem. 83 (12) (2013) 2352–2360, https://doi.org/10.1134/S107036321312027X.

[30] M. Turkyilmaz, G. Uluçam, Ş. Aktaş, S.E. Okan, Synthesis and characterization of new N-heterocyclic carbene ligands: 1, 3-Bis (acetamide) imidazole-3-ium bromide and 3-(acetamide)-1-(3-aminopropyl)-1H-imidazole-3-ium bromide, J. Mol. Struct. 1136 (2017) 263–270, https://doi.org/10.1016/j.molstruc.2017.02.022.

[31] K. Sayin, D. Karakaş, Structural, spectral, NLO and MEP analysis of the [MgO2Ti2 (OPri) 6],[MgO2Ti2 (OPri) 2 (acac) 4] and [MgO2Ti2 (OPri) 2 (bzac) 4] by DFT method, Spectrochim. Acta Mol. Biomol. Spectrosc. 144 (2015) 176–182, https://doi.org/10.1016/j.saa.2015.02.086.

[32] G. Uluçam, Ş.E. Okan, Ş. Aktaş, B. Yentürk, New Schiff-base ligands containing thiophene terminals: synthesis, characterization and biological activities, J. Mol. Struct. 1230 (2021), 129941, https://doi.org/10.1016/j.molstruc.2021.129941.
[33] K.S. Devi, P. Subramani, S. Parthiban, N. Sundaraganesan, One-pot synthesis, spectroscopic characterizations, quantum chemical calculations, docking and cytotoxicity of 1-((dibenzylamino) methyl) pyrrolidine-2, 5-dione, J. Mol. Struct. 1203 (2020), 127403, https://doi.org/10.1016/j.molstruc.2019.127403.
[34] G. Uluçam, U. Bagcı, A.Ş. Yılmaz, B. Yentürk, Schiff-base ligands containing phenanthroline terminals: synthesis, characterization, biological activities and molecular docking study, Spectrochim. Acta Mol. Biomol. Spectrosc. 279 (2022), 121429, https://doi.org/10.1016/j.saa.2022.121429.
[35] T. Mosmann, Rapid colorimetric assay for cellular growth and survival: application to proliferation and cytotoxicity assays, J. Immunol. Methods 65 (1–2) (1983) 55–63, https://doi.org/10.1016/0022-1759(83)90303-4.
[36] S. Boy, A. Aras, F. Türkan, O. Akyıldırım, M. Beytur, H. Sedef Karaman, S. Manap, H. Yüksek, Synthesis, spectroscopic analysis, and in vitro/in silico biological studies of novel piperidine derivatives heterocyclic schiff-mannich base compounds, Chem. Biodivers. 18 (12) (2021), e2100433, https://doi.org/10.1002/cbdv.202100433.
[37] Y. Zhen, X. Shan, Y. Li, Z. Lin, L. Zhang, C. Lai, F. Qin, Exploring the Potential Mechanism of Radix Astragali against Ischemic Stroke Based on Network Pharmacology and Molecular Docking, Phytomedicine Plus, 2022, 100244, https://doi.org/10.1016/j.phyplu.2022.100244.
[38] V. Yadav, A. Krishnan, M.S. Baig, M. Majeed, M. Nayak, D. Vohora, Decrypting the interaction pattern of Piperlongumine with calf thymus DNA and dodecamer d (CGCGAATTCGCG) 2 B-DNA: biophysical and molecular docking analysis, Biophys. Chem. 285 (2022), 106808, https://doi.org/10.1016/j.bpc.2022.106808.
[39] K. Anju, G. Shoba, A. Sumita, M.D. Balakumaran, R. Vasanthi, R. Kumaran, Interaction of acridinedione dye with a globular protein in the presence of site selective and site specific binding drugs: photophysical techniques assisted by molecular docking methods, Spectrochim. Acta Mol. Biomol. Spectrosc. 258 (2021), 119814, https://doi.org/10.1016/j.saa.2021.119814.
[40] K. Crampon, A. Giorkallos, M. Deldossi, S. Baud, L.A. Steffenel, Machine-learning methods for ligand–protein molecular docking, Drug Discov. Today (2021), https://doi.org/10.1016/j.drudis.2021.09.007.
[41] O. Trott, A.J. Olson, AutoDock Vina, Improving the speed and accuracy of docking with a new scoring function, efficient optimization, and multithreading, J. Comput. Chem. 31 (2) (2010) 455–461, https://doi.org/10.1002/jcc.21334.
[42] G.M. Morris, R. Huey, W. Lindstrom, M.F. Sanner, R.K. Belew, D.S. Goodsell, A.J. Olson, AutoDock 4 and AutoDockTools 4: automated docking with selective receptor flexibility, J. Comput. Chem. 30 (16) (2009) 2785–2791, https://doi.org/10.1002/jcc.21256.
[43] J. Stamos, M.X. Sliwkowski, C. Eigenbrot, Structure of the epidermal growth factor receptor kinase domain alone and in complex with a 4-anilinoquinazoline inhibitor, J. Biol. Chem. 277 (48) (2002) 46265–46272, https://doi.org/10.1074/jbc.M207135200.
[44] M. Chalkha, A.A. el Hassani, A. Nakkabi, B. Tüzün, M. Bakhouch, A.T. Benjelloun, M. Sfaira, M. Saadi, L. El Ammari, M. El Yazidi, Crystal structure, Hirshfeld surface and DFT computations, along with molecular docking investigations of a new pyrazole as a tyrosine kinase inhibitor, J. Mol. Struct. 1273 (2023), 134255, https://doi.org/10.1016/j.molstruc.2022.134255.
[45] V.H. Masand, V. Rastija, PyDescriptor: a new PyMOL plugin for calculating thousands of easily understandable molecular descriptors, Chemometr. Intell. Lab. Syst. 169 (2017) 12–18, https://doi.org/10.1016/j.chemolab.2017.08.003.
[46] W.L. DeLano, The PyMOL Molecular Graphics System, 2002.
[47] E.F. Pettersen, T.D. Goddard, C.C. Huang, G.S. Couch, D.M. Greenblatt, E.C. Meng, T.E. Ferrin, UCSF Chimera—a visualization system for exploratory research and analysis, J. Comput. Chem. 25 (13) (2004) 1605–1612, https://doi.org/10.1002/jcc.20084.
[48] M.F. Adasme, K.L. Linnemann, S.N. Bolz, F. Kaiser, S. Salentin, V.J. Haupt, M. Schroeder, PLIP 2021: expanding the scope of the protein–ligand interaction profiler to DNA and RNA, Nucleic Acids Res. 49 (W1) (2021) W530–W534, https://doi.org/10.1093/nar/gkab294.
[49] C.A. Lipinski, Lead-and drug-like compounds: the rule-of-five revolution, Drug Discov. Today Technol. 1 (4) (2004) 337–341, https://doi.org/10.1016/j.ddtec.2004.11.007.
[50] F. Cheng, W. Li, Y. Zhou, J. Shen, Z. Wu, G. Liu, P.W. Lee, Y. Tang, admetSAR: a Comprehensive Source and Free Tool for Assessment of Chemical ADMET Properties, ACS Publications, 2012, https://doi.org/10.1021/ci300367a.
[51] Z. Demircioğlu, Ç.A. Kaştaş, O. Büyükgüngör, Theoretical analysis (NBO, NPA, Mulliken Population Method) and molecular orbital studies (hardness, chemical potential, electrophilicity and Fukui function analysis) of (E)-2-((4-hydroxy-2-methylphenylimino) methyl)-3-methoxyphenol, J. Mol. Struct. 1091 (2015) 183–195, https://doi.org/10.1016/j.molstruc.2015.02.076.
[52] Q.S. Obu, H. Louis, J.O. Odey, I.J. Eko, S. Abdullahi, T.N. Ntui, O.E. Offiong, Synthesis, spectra (FT-IR, NMR) investigations, DFT study, in silico ADMET and Molecular docking analysis of 2-amino-4-(4-aminophenyl) thiophene-3-carbonitrile as a potential anti-tubercular agent, J. Mol. Struct. 1244 (2021), 130880, https://doi.org/10.1016/j.molstruc.2021.130880.
[53] K.E. Anwer, G.H. Sayed, R.M. Ramadan, Synthesis, spectroscopic, DFT calculations, biological activities and molecular docking studies of new isoxazolone, pyrazolone, triazine, triazole and amide derivatives, J. Mol. Struct. 1256 (2022), 132513, https://doi.org/10.1016/j.molstruc.2022.132513.
[54] W.E. Śmiszek-Lindert, E. Chełmecka, O. Lindert, A. Dudzińska, I. Kaczmarczyk-Sedlak, Towards a better comprehension of interactions in the crystalline N-acetylbenzylamine and its sulphur analogue N-benzyl-ethanethioamide. IR, Raman, DFT studies and Hirshfeld surfaces analysis, Spectrochim. Acta Mol. Biomol. Spectrosc. 201 (2018) 328–338, https://doi.org/10.1016/j.saa.2018.05.021.
[55] F. El Kalai, K. Karrouchi, C. Baydere, S. Daoui, M. Allali, N. Dege, N. Benchat, S.A. Brandan, Synthesis, crystal structure, spectroscopic studies, NBO, AIM and SQMFF calculations of new pyridazinone derivative, J. Mol. Struct. 1223 (2021), 129213, https://doi.org/10.1016/j.molstruc.2020.129213.
[56] Y. Umar, Experimental (FT-IR, FT-Raman, and NMR) and DFT studies of the structures and spectral properties of diphenylcarbazone and diphenylthiocarbazone, J. Mol. Struct. 1264 (2022), 133230, https://doi.org/10.1016/j.molstruc.2022.133230.
[57] Y. Sheena Mary, Y. Shyma Mary, G. Serdaroglu, S. Kaya, B. Sarojini, H. Umamahesvari, B. Mohan, Conformational Analysis, Spectroscopic Insights, Chemical Descriptors, ELF, LOL and Molecular Docking Studies of Potential Pyrimidine Derivative with Biological Activities, Polycyclic Aromatic Compounds, 2021, pp. 1–11, https://doi.org/10.1080/10406638.2021.1924803.
[58] O. Unsalan, B. Szolnoki, A. Toldy, G. Marosi, FT-IR spectral, DFT studies and detailed vibrational assignment on N, N′, N ″-tris (2-aminoethyl)-phosphoric acid triamide, Spectrochim. Acta Mol. Biomol. Spectrosc. 98 (2012) 110–115, https://doi.org/10.1016/j.saa.2012.08.050.
[59] A. Ouaket, A. Chraka, I. Raissouni, M.A. El Amrani, M. Berrada, N. Knouzi, Synthesis, spectroscopic (13C/1H-NMR, FT-IR) investigations, quantum chemical modelling (FMO, MEP, NBO analysis), and antioxidant activity of the bis-benzimidazole molecule, J. Mol. Struct. 1259 (2022), 132729, https://doi.org/10.1016/j.molstruc.2022.132729.
[60] A. Abdou, O.A. Omran, A. Nafady, I.S. Antipin, Structural, spectroscopic, FMOs, and non-linear optical properties exploration of three thiacaix (4) arenes derivatives, Arab. J. Chem. 15 (3) (2022), 103656, https://doi.org/10.1016/j.arabjc.2021.103656.
[61] G. Ulucam, B. Yenturk, S.E. Okan, S. Aktas, Double vanadyl-carrying phenanthroline complexes: template synthesis and DFT study, Chem. Pap. 74 (6) (2020) 1881–1889, https://doi.org/10.1007/s11696-019-01037-9.
[62] A. Vela, J.L. Gazquez, A relationship between the static dipole polarizability, the global softness, and the fukui function, J. Am. Chem. Soc. 112 (4) (1990) 1490–1492, https://doi.org/10.1021/ja00160a029.
[63] Y.S. Mary, Y.S. Mary, DFT analysis and molecular docking studies of the cocrystals of sulfathiazole-theophylline and sulfathiazole-sulfanilamide, Polycycl. Aromat. Comp. 42 (6) (2022) 3809–3820, https://doi.org/10.1080/10406638.2021.1873809.
[64] A. Boshaala, M.A. Said, E.A. Assirey, Z.S. Alborki, A.A. AlObaid, A. Zarrouk, I. Warad, Crystal structure, MEP/DFT/XRD, thione⇔ thiol tautomerization, thermal, docking, and optical/TD-DFT studies of (E)-methyl 2-(1-phenylethylidene)-hydrazinecarbodithioate ligand, J. Mol. Struct. 1238 (2021), 130461, https://doi.org/10.1016/j.molstruc.2021.130461.
[65] H. Kargar, M. Fallah-Mehrjardi, R. Behjatmanesh-Ardakani, K.S. Munawar, M. Ashfaq, M.N. Tahir, Diverse coordination of isoniazid hydrazone Schiff base ligand towards iron (III): synthesis, characterization, SC-XRD, HSA, QTAIM, MEP, NCI, NBO and DFT study, J. Mol. Struct. 1250 (2022), 131691, https://doi.org/10.1016/j.molstruc.2021.131691.

[66] S. Demir, S. Cakmak, N. Dege, H. Kutuk, M. Odabasoglu, R.A. Kepekci, A novel 3-acetoxy-2-methyl-N-(4-methoxyphenyl) benzamide: molecular structural describe, antioxidant activity with use X-ray diffractions and DFT calculations, J. Mol. Struct. 1100 (2015) 582–591, https://doi.org/10.1016/j.molstruc.2015.08.014.
[67] A.K. Farag, B.S. Ahn, J.S. Yoo, R. Karam, E.J. Roh, Design, synthesis, and biological evaluation of pseudo-bicyclic pyrimidine-based compounds as potential EGFR inhibitors, Bioorg. Chem. (2022), 105918, https://doi.org/10.1016/j.bioorg.2022.105918.
[68] E. Zarenezhad, M. Farjam, A. Iraji, Synthesis and biological activity of pyrimidines-containing hybrids: focusing on pharmacological application, J. Mol. Struct. 1230 (2021), 129833, https://doi.org/10.1016/j.molstruc.2020.129833.
[69] J. Woodburn, The epidermal growth factor receptor and its inhibition in cancer therapy, Pharmacol. Therapeut. 82 (2–3) (1999) 241–250, https://doi.org/10.1016/S0163-7258(98)00045-X.
[70] P. Traxler, P. Furet, Strategies toward the design of novel and selective protein tyrosine kinase inhibitors, Pharmacol. Therapeut. 82 (2–3) (1999) 195–206, https://doi.org/10.1016/S0163-7258(98)00044-8.
[71] H. Medetalibeyoğlu, F. Türkan, S. Manap, E. Bursal, M. Beytur, A. Aras, O. Akyıldırım, G. Kotan, Ö. Gürsoy-Kol, H. Yüksek, Synthesis and acetylcholinesterase enzyme inhibitory effects of some novel 4, 5-Dihydro-1 H-1, 2, 4-triazol-5-one derivatives; an in vitro and in silico study, J. Biomol. Struct. Dyn. (2022) 1–9, https://doi.org/10.1080/07391102.2022.2066021.
[72] Y.S. Mary, Y.S. Mary, K. Resmi, V.S. Kumar, R. Thomas, B. Sureshkumar, Detailed quantum mechanical, molecular docking, QSAR prediction, photovoltaic light harvesting efficiency analysis of benzil and its halogenated analogues, Heliyon 5 (11) (2019), e02825, https://doi.org/10.1016/j.heliyon.2019.e02825.
[73] S. Aliwaini, B. Abu Thaher, I. Al-Masri, N. Shurrab, S. El-Kurdi, D. Schollmeyer, B. Qeshta, M. Ghunaim, R. Csuk, S. Laufer, Design, synthesis and biological evaluation of novel pyrazolo [1, 2, 4] triazolopyrimidine derivatives as potential anticancer agents, Molecules 26 (13) (2021) 4065, https://doi.org/10.3390/molecules26134065.
[74] Y. Haddad, M. Remes, V. Adam, Z. Heger, Toward structure-based drug design against the epidermal growth factor receptor (EGFR), Drug Discov. Today 26 (2) (2021) 289–295, https://doi.org/10.1016/j.drudis.2020.10.007.